Experimental Mechanics
https://doi.org/10.1007/s11340-024-01109-2

RESEARCH PAPER

Biomechanical Hand Model: Modeling and Simulating the Lateral Pinch Movement

A.F. Lemos[1,2] · L.A. Rodrigues da Silva[3] · B.V. Nagy[1] · P.N. Barroso[4,5] · C.B.S. Vimieiro[2,4]

Received: 11 February 2024 / Accepted: 19 August 2024

Abstract

Background Hand movements are crucial in daily activities, sparking extensive interest and research in biomechanical models. While existing models offer valuable insights, their complexity and processing costs may limit their suitability for all applications, sometimes impeding research efficiency.

Objectives This study aimed to develop a biomechanical model of the human hand for analyzing the physiology of lateral pinch movement. Unlike conventional methodologies, this approach focuses on delivering a computationally efficient model while incorporating the trapeziometacarpal joint into the analysis.

Methods The model, which operates in a multibody environment, simulates lateral pinching movement by applying external time-varying torques to digit joints, emulating musculature, tendons, and ligaments. Torque estimation was achieved through the Euler-Lagrange approach. The model generates animated representations of the movement, aiding pathology identification and outputting dynamic variables. The model's was validated through data acquired from asymptomatic subjects via an OptiTrack system.

Results The average disparity between the expected and obtained joint angular displacements was **6.06 %** and **1.90 %** during validation and verification stages, suggesting high fidelity in the model performance. Correlation analysis revealed strong positive linear relationships and robust correlations between the obtained and expected configuration data. Model-generated pinch postures closely resembled expected physiological patterns, with results falling within the range for asymptomatic individuals documented in the scientific literature.

Conclusion The system efficiently analyzes dynamic variables at a low computational cost, offering animated representations for pathology identification. The model's potential for rehabilitation solutions and adaptability, coupled with its accuracy and versatility, make it an asset for advancing hand biomechanics research.

Keywords Computational model · Hand model · Upper limb · Pinch movement · Biomechanics

Introduction

The human hand is able to perform complex tasks with dexterity [1]. This is due to the human thumb structure, which contains the trapeziometacarpal joint (TMCJ), enabling digital opposition through lateral and rotational movements of the thumb [2]. As a result, the opposition allows the human hand to perform palmar grasping, along with lateral, tripod, and cylindrical pinching, which are movements involved in approximately 90% of the daily upper limb activities of asymptomatic individuals [1].

The versatility of the hand arises from the complexity of its structure and refined control. In total, 27 bones constitute the hand anatomy [3], along with the ligament system, muscle function, tendons, sensory properties of the skin, and nervous network, which assist in the execution of 23 degrees of freedom (DOFs) and individual movement of each finger [4].

Hand movements play a fundamental role in various daily activities and have led to significant interest in these activities in diverse fields, including neuroscience and robotics [5]. The literature includes numerous studies on biomechanical models related to hand movement, with several noteworthy examples. These models have been employed in various

L.A. Rodrigues da Silva, B.V. Nagy, P.N. Barroso and C.B.S. Vimieiro contributed equally to this work.

Extended author information available on the last page of the article

Published online: 19 September 2024

applications, such as the analysis of hand biomechanics during grasp movements [4, 6, 7] and in-depth analysis of specific joints [8].

Biomechanical models are also involved in tasks such as aiding in the design of rehabilitation devices, prosthetics and orthoses and evaluating their effectiveness [4, 9–12]. These models translate the physiological behavior of organs associated with such devices and predict their responses under specific predetermined conditions [9, 13].

Although these works have made valuable contributions, they may not be suitable for all applications. Some of these do not emulate the TMCJ movement [9, 10]. Others are solely dedicated to representing the TMCJ [8]. Despite providing detailed insights, certain models entail a substantial processing cost for simulations [4]. Regardless of the advancements in current processing capabilities, computational model design still considers computational expense a crucial factor. Model complexity is not always essential and can sometimes impede research due to limitations in processing time.

Furthermore, specific models are purely kinematic in nature [6, 7]. Although kinematic models offer advantages in terms of simplicity and reduced processing expenses, their applicability varies depending on the context. For studies involving the deformation of external bodies, such as in the design and evaluation of prosthetics and orthoses, a dynamic analysis becomes indispensable for assessing outcomes, including the behavior of the device during movement. Therefore, computational models designed for such applications should integrate dynamic components to account for body interactions and facilitate the incorporation of flexible or deformable elements into the analysis.

In light of these findings, this study presents a biomechanical model of the human hand, that enables the analysis of the physiology of lateral pinching movement. The system employs dynamic principles, ensuring computational efficiency while incorporating the TMCJ into the analysis. Furthermore, the model's simulation can output dynamic and kinematic variables derived from the model and generate a hand movement animation that aids in identifying potential pathologies. The resulting pinch postures were closely aligned with physiological patterns. The validation of the biomechanical model involved comparing the simulated angular position of the TMCJ to the literature, which supported the model's fidelity. Furthermore, the system exhibited a low computational cost.

Theoretical Basis

The hand plays a vital role in our daily activities, acting as a remarkable tool that allows us to interact with the environment. With their intricate structure, the fingers consist of segments called phalanges and metacarpals. Each finger, except the thumb, comprises three phalanges: the proximal, the middle, and the distal phalanx. The thumb, on the other hand, has two phalanges, the proximal and distal phalanges. The metacarpal bones form the palm of the hand and connect the fingers to the wrist. Figure 1(b) illustrates the hand segments along the main joints.

Finger joints are responsible for the incredible range of movements our hands can achieve. At the base of each finger, the metacarpophalangeal (MCP) joint allows flexion and extension movements. Moving further along the finger, we find the proximal interphalangeal joint (PIP), which permits flexion and extension between the proximal and middle phalanges. Finally, at the tip of the finger, the distal interphalangeal joint (DIP) is involved, enabling flexion and extension between the middle and distal phalanges [3, 4, 14, 15], as shown in Fig. 1(b).

As indicated by the graph in Fig. 1(a), the fingers also possess the ability to perform abduction-adduction and flexion-extension movements. Abduction refers to the movement of the fingers away from the midline of the hand, such as when the fingers are spread apart. Adduction, on the other hand, involves bringing the fingers back toward the midline, allowing them to come together. Flexion is the bending movement that decreases the angle between the bones of the joint, while extension is the opposite movement that increases the angle and straightens the joint.

These complex movements of abduction-adduction and flexion-extension enable our hands to grasp objects, manipulate tools, write, play musical instructions, and perform countless other daily tasks with precision and finesse. The hand's remarkable anatomy, including the phalange and metacarpal segments, along with the intricate network of joints, grants us the ability to carry out a wide range of activities that enhance our lives. The lateral pinch Fig. 1(c), a fundamental dexterity feature of the human hand, plays a pivotal role in daily life, enabling us to perform precise tasks that involve holding, gripping, and manipulating objects with fins and control.

Methods

The model was developed in a multibody environment using Altair MotionView^{TM} software and simulates lateral pinch movements by applying external time-varying torques to the digit joints. These torques emulate the efforts exerted by the upper limb musculature, tendons, and ligaments during this motion. The model takes these torque signals as inputs. The torque equations used to estimate these torque signals are also derived in the present work through the Euler-Lagrange formulation and were applied for model validation. The equations take hand joint displacements as input, and the

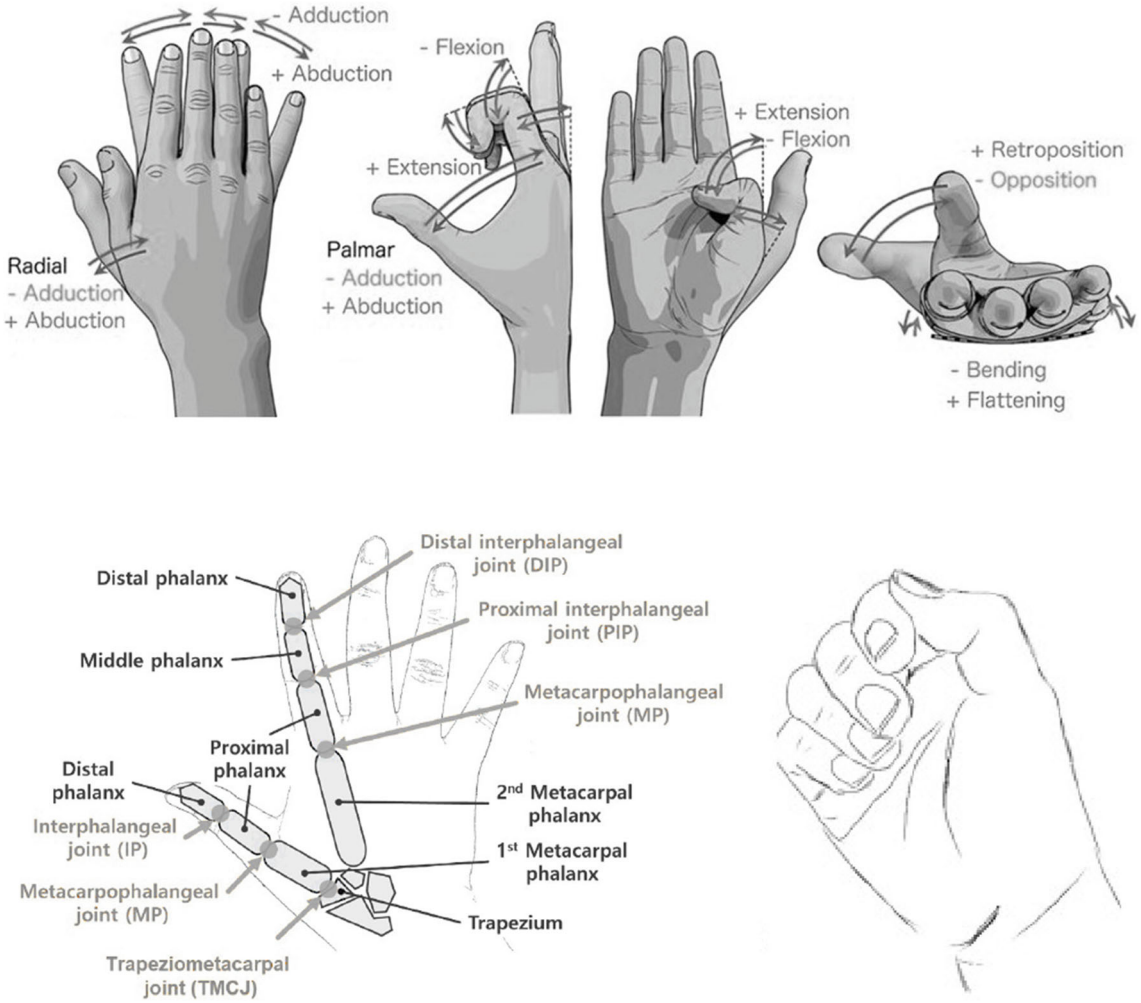

Fig. 1 Theoretical basis. a) Digits of abduction-adduction and flexion-extension movements [16]. b) Major joints and segments of the thumb and index finger [17]. c) Lateral pinch posture [18]

methodology for acquiring these signals is included within the validation process to ensure the model's functionality.

This section outlines the methods and procedures employed in our study, from computational model design to validation. The approach is described in detail in several key subsections. First, the subsection "Topology of the Model" provides a comprehensive overview of the model's structure, including a description of the graphic model Section "Graphic model" and joint elements Section "Joints". The dynamic modeling Section "Dynamic Modeling" aspect is explored through the characterization of external torque equations using the Euler-Lagrange formulation. A description of the torque equation's inputs Section "Inputs of the torque equations" and dynamic analysis Section "Dynamic Analysis" are also presented in this subsection. The subsection "Experimental Analysis" outlines the data acquisition from subjects conducted using the OptiTrack system in an *in-vivo* experiment. These terms are further divided into Sections "Subjects" and "Experimental setup". The final subsection consists of Section "Model validation".

Topology of the Model

The proposed computational model aims to simulate lateral pinch movement. Altair MotionView^{TM} was selected as the multibody environment for developing the model. Altair MotionView^{TM} is a comprehensive tool within the Altair HyperWorks suite was designed specifically for creating and analyzing multi-body dynamic models. This allows users to build detailed mechanical models, simulate their dynamic behavior, and analyze the results. This software is widely used in various engineering fields, including biomechanics, to study the movement and interaction of complex systems.

The main elements of the system are the graphic model of the hand Section "Graphic model"; joint elements for body interconnections Section "Joints"; and external torques

applied to the joints to emulate the effects of the efforts performed by the muscles, tendons and ligaments of the human hand during the pinch movement. These time-varying torque signals serve as the expected inputs to the model, which will produce time-varying displacements measured from the model joints and generate an animation of the hand movement induced by the application of torques. Figure 2 presents a block diagram that illustrates the topology of the hand model, including the inputs and outputs of the model.

Validating the model requires pairs of inputs (time-varying torques) and corresponding expected outputs (joint kinematics data). However, such data are not available in the literature. Direct measurement of these torques from participants during an experiment would be highly invasive, requiring multiple dynamometers that could interfere with the natural pinch movement. Therefore, an alternative validation method was introduced in this study. The torques were modeled using the Euler-Lagrange formulation (refer to section "Dynamic Analysis"), which requires joint kinematics as input. These kinematic data were obtained from participants through experimental analysis, as detailed in section "Experimental Analysis".

Graphic Model

The graphic hand model consists of a computer aided design (CAD) model obtained from Ersin on GrabCAD [19]. Although the original model is titled the "Tibial Intramedullary Nail," it contains comprehensive human skeletal and soft tissue meshes, including those relevant to the upper limb. Given that the aim of the model is to study lateral pinch movement, body segments unrelated to the right upper limb were discarded. The hand segments in the model already contained specific anthropometric measurements and masses, providing a detailed representation of the anatomical characteristics of each segment. The computational model of the right upper limb is composed of thirty-two rigid bodies, which comprise fourteen phalange bones with soft tissues; five metacarpal, eight carpal, ulna, radius and humerus bones; one soft tissue embracing the first metacarpal; and one soft tissue enclosing the dorsal and palm surfaces. The scales of the original model were modified to eliminate disproportions. Additionally, to ensure that each finger underwent planar movement, the centers of mass (CMs) of the segments were aligned in a single plane. The modified model was imported into MotionView^{TM}, and the hand segments were modeled as rigid bodies.

Joints

During lateral pinch movement, joints from the index to the small fingers execute mainly flexion-extension movements. Therefore, as a model simplification, the adduction-abduction movement direction was neglected due to its low significance during this movement. Thus, the distal interphalangeal (DIP), middle interphalangeal (PIP), and metacarpophalangeal (MCP) joints of these digits were designed as single rotational degree-of-freedom joints in the flexion-extension movement direction.

Similarly, thumb interphalangeal (IP) and metacarpophalangeal (MCP) joint movements were constrained to one DOF and modeled as single rotational degree-of-freedom joints, allowing flexion/extension movement. The TMCJ was modeled as a universal joint, except with movement constrained to one DOF. Specifically, the origin of the universal joint was set at the center of the base of the first metacarpal bone (midpoint of the line $TMCV-TMCD$), the shaft direction was aligned toward the center of mass of the first metacarpal (the same direction as the metacarpophalangeal joint), and the crosspin direction was aligned with the $Z-$ *axis* direction of Fig. 6. These settings constrained the TMCJ movement to the adduction/abduction direction defined by

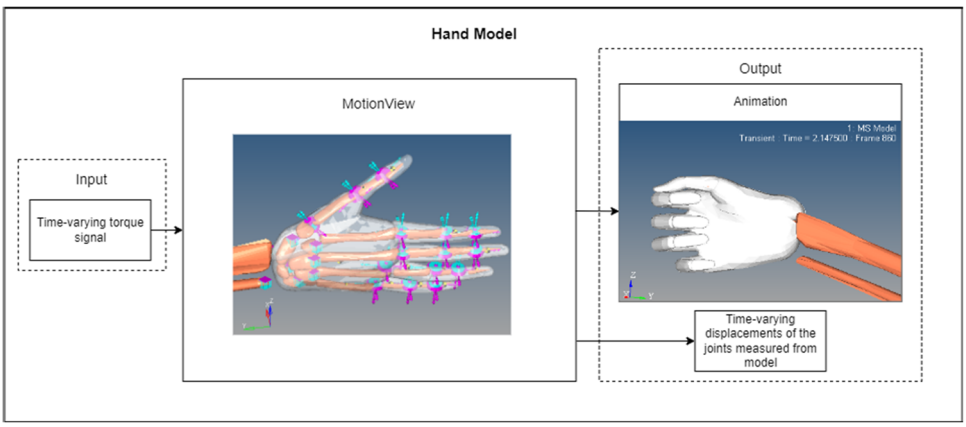

Fig. 2 Block diagram illustrating the topology of the hand model, including inputs and outputs of the model

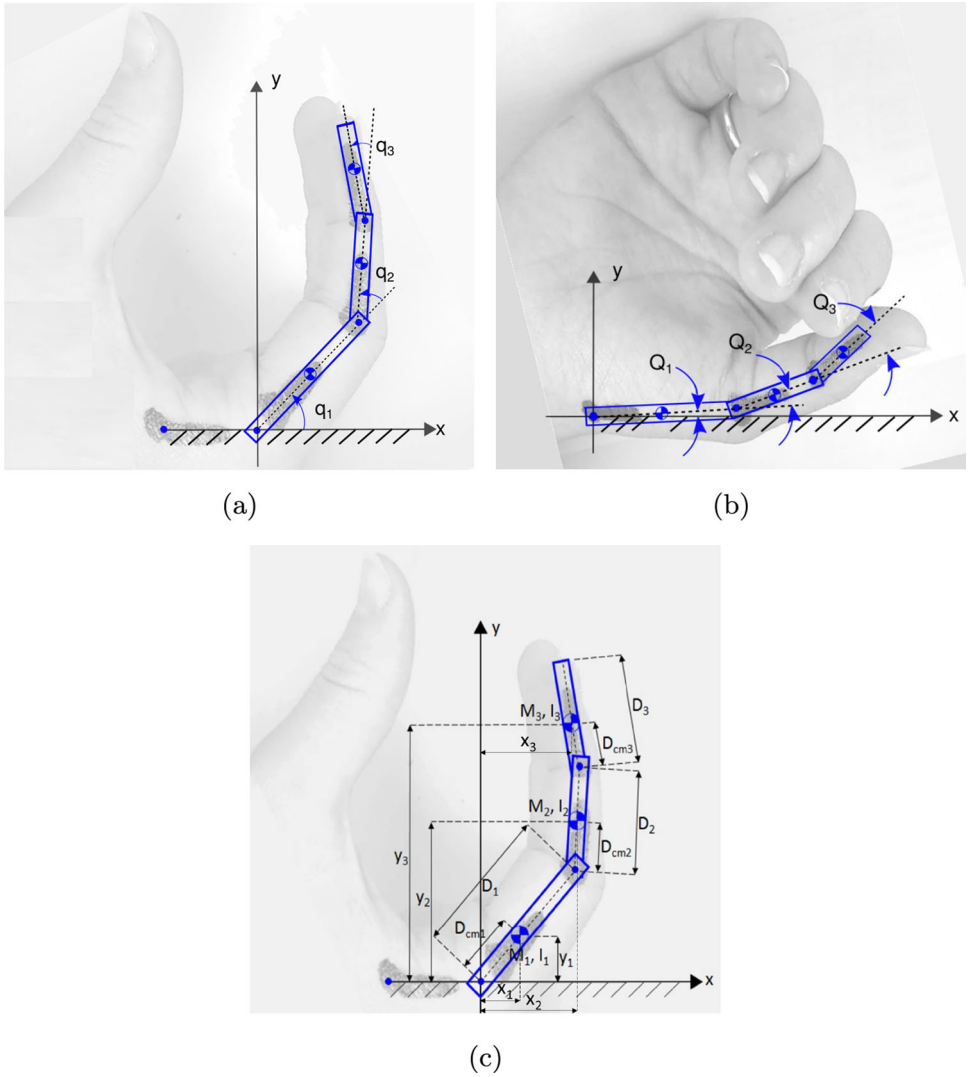

Fig. 3 Digit configuration associated with 3 degree-of-freedom planar manipulators

vector V1, as per Barroso's methodology [1], which is further described as the direction of the vector $\vec{V}_1$ in section "Experimental setup". The remaining body connections were defined as fixed joints.

The body connections consist of twenty-nine joints, including fourteen fixed joints, fourteen single rotational degree-of-freedom joints, and one universal joint. Figure 4(a) shows a magnification of the model displaying the rotational, universal joint, and a few fixed joints. The model included fifteen DOFs, which allowed flexion-extension of the intra-phalangeal and metacarpophalangeal segments and abduction-adduction of the trapeziometacarpal joint.

Dynamic Modeling

The simulation of pinch movement in multibody software demands time-varying torques applied by external sources, such as muscles, tendons and ligaments, to each joint. Since, to the best of the author's knowledge, the scientific literature does not present these torque signals, they were characterized in the present study. Such characterization is based on the Euler-Lagrange approach [20], for which the torques are related to the mechanical configurations of the joints. The Euler-Lagrange equation is presented in equation (1), where $\vec{\tau}$ is the torque vector applied by external sources, L is the system Lagrangian, and $\vec{q}$ is the position configuration vector, and $\dot{\vec{q}}$ is the velocity configuration vector.

$$\vec{\tau} = \frac{\partial}{\partial t}\frac{\partial L}{\partial \dot{\vec{q}}} - \frac{\partial L}{\partial \vec{q}} \tag{1}$$

The first step in using the Euler-Lagrange method is to determine the body configurations. For lateral pinch movement, the digits perform planar motion. Based on this consideration, each finger is modeled as a planar manipulator

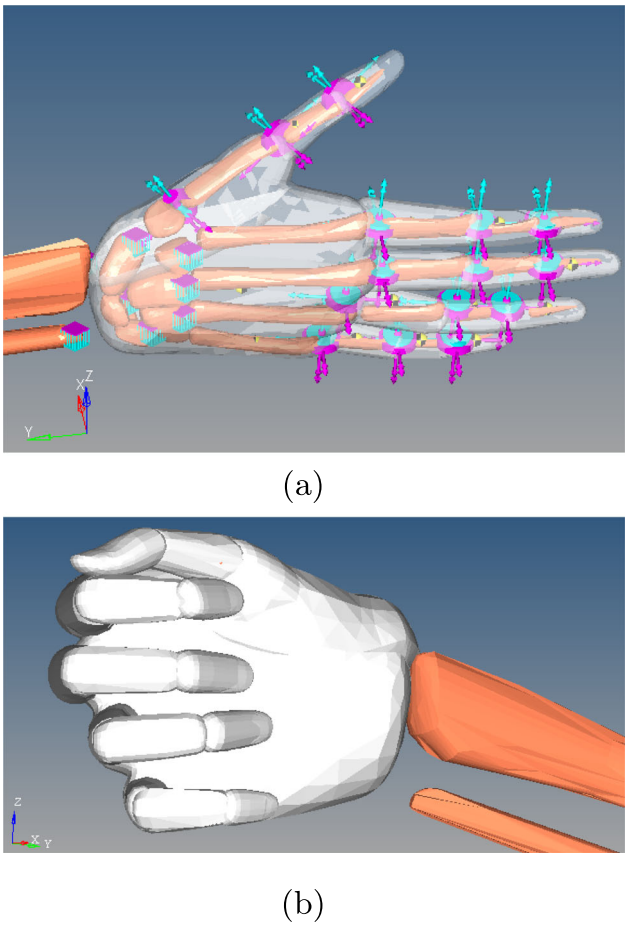

Fig. 4 Adapted graphic model used as the basis for project execution. a) Graphic model and joint elements; b) Computational model in the lateral pinch posture

with three DOFs. From this point, the variables related to the digit segments are enumerated from the proximal to the distal positions in ascending order. The thumb is represented by configurations Q_1, Q_2, and Q_3, corresponding to the angular positions of the trapeziometacarpal, metacarpophalangeal, and interphalangeal joints, respectively. These angles denote the positional relationships of the first metacarpal, proximal phalanx, and distal phalanx with respect to their preceding segment, as illustrated in Fig. 3(b). In contrast, the remaining digits adopted the same configuration as the index, with q_1, q_2, and q_3 representing the angular displacements of the metacarpophalangeal, proximal interphalangeal, and distal interphalangeal joints, respectively. These angles signify the differences in position between the proximal, medial, and distal phalanges concerning their preceding segment, as shown in Fig. 3(a). The configuration parameters are illustrated in Fig. 3(c), in which D_1, D_2 and D_3 are the segments' lengths and D_{cm1}, D_{cm2} and D_{cm3} are the CM positions in relation to the bases of the segments.

Characterization of the Joint Torques

As presented in equation (1) the torque calculation for each joint demands the characterization of the Lagrangian function. From [20], this function is calculated from the total kinetic and potential energies, as presented in equation (2), where K_1, K_2 and K_3 are the segments' kinetic energies and V_1, V_2 and V_3 are the segments' potential energies.

$$L(\vec{q},\dot{\vec{q}}) = (K_1(\vec{q},\dot{\vec{q}}) + K_2(\vec{q},\dot{\vec{q}}) + K_3(\vec{q},\dot{\vec{q}})) - (V_1(\vec{q}) + V_2(\vec{q}) + V_3(\vec{q})) \tag{2}$$

The expressions for kinetic and potential energies as functions of the mechanical configurations are presented in equations (3) to (8), where M_1, M_2 and M_3 are the masses of the segments; $\dot{x_1}$, $\dot{x_2}$, $\dot{x_3}$, $\dot{y_1}$, $\dot{y_2}$, and $\dot{y_3}$ are the velocity coordinates of the centers of mass of the segments; I_1, I_2 and I_3 are the moments of inertia measured around the center of mass; g is the gravitational acceleration; y_1, y_2 and y_3 are the y coordinates of the centers of mass of the segments; and x_1, x_2 and x_3 are the x coordinates of the centers of mass of the segments. Figure 3(c) presents a diagram that illustrates the dimension parameters and masses indicated in the equations.

$$K_1 = \frac{1}{2} \cdot M_1 \cdot (\dot{x_1}^2 + \dot{y_1}^2) + \frac{1}{2} \cdot I_1 \cdot \dot{q_1}^2 \tag{3}$$

$$V_1 = M_1 \cdot g.y_1 \tag{4}$$

$$K_2 = \frac{1}{2} \cdot M_2 \cdot (\dot{x_2}^2 + \dot{y_2}^2) + \frac{1}{2} \cdot I_2 \cdot (\dot{q_1} + \dot{q_2})^2 \tag{5}$$

$$V_2 = M_2 \cdot g \cdot y_2 \tag{6}$$

$$K_3 = \frac{1}{2} \cdot M_3 \cdot (\dot{x_3}^2 + \dot{y_3}^2) + \frac{1}{2} \cdot I_3 \cdot (\dot{q_1} + \dot{q_2} + \dot{q_3})^2 \tag{7}$$

$$V_3 = M_3 \cdot g \cdot y_3 \tag{8}$$

Substituting the kinetic and potential energy expressions, equations (4) to (8), into the Euler-Lagrange expression, equations (2), the torques for each joint are obtained. These torques are presented in the Appendix A in equations (10) to (12).

Table 1 presents the anthropometric parameters and masses of each segment of the computational hand model, as defined by the CAD model [19]. These dimensional parameters and masses are used in equations (10) to (12). The moments of inertia are determined by approximating the segments as cylindrical geometries.

In constructing the torque equations via the Euler-Lagrange formulation, the gravitational potential energy was included to preserve the canonical form of the equations (Appendix A). However, for the specific configurations

Table 1 Anthropometric parameters and masses of the computational hand model

Digit	Segment	Segment length (D) [mm]	Center of mass (D_{cm}) [mm]	Diameter (d) [mm]	Mass (M) [g]
Thumb	Metacarpal	35.3	17.7	18.5	68.8
	Proximal Phalanx	21.2	6.4	12.1	24.1
	Distal Phalanx	22.2	7.5	10.5	13.3
Index	Metacarpal	54.5	25.4	5.7	11.8
	Proximal Phalanx	29.3	9.7	12.8	42.5
	Middle Phalanx	19.3	6.3	10.6	16.1
	Distal Phalanx	17.7	5.2	6.2	8.5
Middle	Metacarpal	57.7	28.5	7.3	11.7
	Proximal Phalanx	27.8	9.5	12.6	33.8
	Middle Phalanx	20.3	6.3	10.5	18
	Distal Phalanx	22.5	8	9.1	11.1
Ring	Metacarpal	48.9	22.3	6.5	10.2
	Proximal Phalanx	32.6	14	12.1	29.4
	Middle Phalanx	14.5	4.6	9.6	13.8
	Distal Phalanx	23.8	12.1	7.7	9.4
Small	Metacarpal	40.4	20.2	5.4	5.8
	Proximal Phalanx	22.3	10.3	10.4	18.6
	Middle Phalanx	16.8	6.8	9.3	10.2
	Distal Phalanx	15.7	5.7	8.6	4.5

and movements analyzed in this study, gravitational effects were considered negligible. Consequently, the gravitational acceleration (g) was set to zero during the simulations to simplify the model without compromising its accuracy for the intended applications.

Inputs of the torque equations

As presented in equations (10) to (12), the kinematic variables, which are time-varying signals of displacement, velocity and acceleration of the configurations, are inputs of the torques. The format of the input dataset is described in section "Experimental Setup", which also includes guidelines for its measurements.

The kinematic data provided as inputs are proportional to the lengths of the digits of the participants under analysis, which differ from the graphic model dimensions. For this reason, the input data are normalized in relation to the dimensions of the model in the data processing module, which aims to process the input data and calculate the torque signals.

MATLAB® software was used as a numerical tool for the data processing module. The joint positions of the graphic model in its initial pose and the lateral pinch posture are used as the initial and final range values of the normalized data. The pinch posture of the model was obtained through iterative tests via kinematic analysis of the computational model. In these tests, the joint positions were modified systematically until the pinch posture was more appropriate for the physiological pattern of the lateral pinch. The pinch posture of the model obtained through iterative tests and used to extract the joint positions for normalizing the input data is presented in Fig. 4(b).

Once the best posture was obtained, the configurations were measured and used as the final values in the normalization process. For the model in the lateral pinch posture, the thumb joint measurement positions were 12.6^o, 21.0^o and 9.2^o for Q_1, Q_2 and Q_3, respectively. For the other digit, the measured positions were 68.8^o, 68.8^o and 57.3^o for q_1, q_2 and q_3, respectively.

The velocity and acceleration signals were further calculated by numerical derivatives of the normalized dataset. The parameters of the biomechanical model are presented in Table 1, and the kinematic data are applied to the torque equations (10) to (12). The torques of each joint of all five fingers are obtained and exported into the biomechanical model, in Altair MotionView™.

Dynamic Analysis

Upon running the computational model on MotionView™, the solver generates an animation of the lateral pinch movement and provides various output variables, which can include measurements of dynamic and kinematic parameters within the system.

The model serves to evaluate the physiology of pinch movements and the final pinch posture by accessing the animation. Additionally, system variables can be quantified through the use of output data, aiding in the identification of potential pathologies.

To validate the model functionality, the model was simulated with experimental kinematic data acquired from the subjects, as described in section "Experimental Analysis". The results of the experiments are presented in section "Results and Discussion".

Experimental Analysis

The torque equations modeled in the present study, equations (10) to (12), use the displacement, velocity and acceleration of the configurations as inputs. To the best of the author's knowledge, examples of kinematic data in the required format are not available in the scientific literature. Therefore, for functionality validation of the system, the simulations were performed using data from subjects as the input of the torque equations, which were acquired using an OptiTrack system as described in this section.

Subjects

To overcome the limitations of the measurement system, the participants in the procedure were chosen based on the length of their index and thumb segments. According to our protocol, the minimum longitudinal length of the hand segments of the participant was greater than 18.0 *mm*. Considering this requirement, a group of six asymptomatic participants was selected from among the eleven initially recruited volunteers. In total, two women ($28-32$ *years*) and four men ($25-31$ *years*) participated. The study was approved by the ethics committee, and each participant signed an informed consent form.

Experimental setup

The experiment was performed at the *BME MOGI MotionLab* [21], which is instrumented with an 18-infrared camera motion capture system (OptiTrack, NaturalPoint Inc., Oregon, USA) [22]. Retro-reflective marker clusters were positioned on the right hand of each participant. The system tracked the markers at a sampling rate of 120 *Hz*. The movements of the volunteer's hand were restricted by a support tripod with free digits, as shown in Fig. 5(a). The participants were asked to execute a lateral pinch movement three times. The best of the three acquisitions was selected as the data under analysis in the present study.

To measure the displacement of the thumb and index finger, eleven reflective markers were placed on the right hand of the participants. The anatomical landmarks for positioning the markers were defined based on the work of Barroso [1, 23]. Figure 5(b) illustrates the marker positions, which consist of the index extremity (IE), index distal interphalangeal (IDIP), index proximal interphalangeal (IPIP), index metacarpophalangeal (IMCP), thumb extremity (TE), thumb interphalangeal (TIP), thumb metacarpophalangeal joint (TMCP), trapeziometacarpal dorsal (TMCD),

(a)

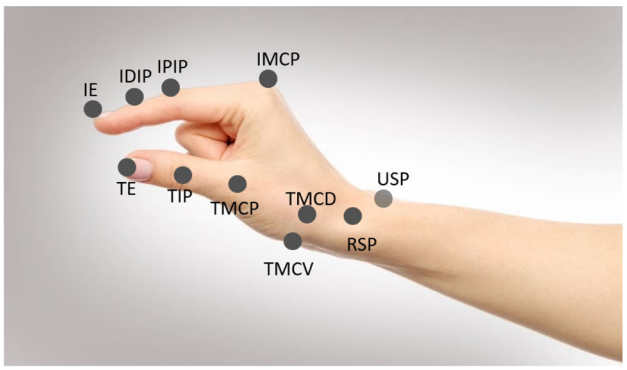

(b)

Fig. 5 Experimental procedure for measuring the position configurations of the participants' hands. a) Measurement setup. b) Position of retro-reflective marker clusters

trapeziometacarpal ventral (TMCV), radial styloid process (RSP), and ulnar styloid process (USP).

The markers IE, IDIP, IPIP, IMCP, and RSP delimitated the phalanges and metacarpal of the index finger and were used to determine its joint positions. The displacements of the configurations were obtained as the difference between the angular positions of consecutive segments in the distal and proximal positions, as illustrated in Fig. 6(b) and (a). Similarly, the markers TE, TIP, and TMCP delimitated the phalanges of the thumb and were used to determine the displacement of the interphalangeal and metacarpal-phalangeal joints. The OptiTrack system acquires the 3D position of each marker. Therefore, for each of these joints, the flexion-extension direction of the movement was determined as the projection of the joint's displacements over the plane that contains the three points that delimitated the segments connected by the joint under analysis.

Following the validated methodology of Barroso (2007) [1, 23], the markers TMCP, TMCD, TMCV, and RSP were used to approximate the movement of the first metacarpal, induced by the angular displacement of the trapeziometacarpal joint. As shown in Fig. 6(c), these markers define a local coordinate system *xyz* used to describe the movement of the first metacarpal. The TMCD and TMCV markers define the *z-axis* direction of the system, while the centers of these two points coincide with the system center. The *x-axis* is determined by the vector product of a unit vector, oriented from the center of the coordinate system to the position of the RSP marker, and the *z-axis*. Subsequently, the *y-axis* is obtained through the vector product of the *x-axis* and the *z-axis*. The $\vec{V}_1$ vector, whose direction is given by the center of *xyz* and the marker TMCP, describes the movement direction of the first metacarpal, whose projection in the *zx* plane corresponds to the abduction-adduction direction of the trapeziometacarpal joint [1, 23].

As a postprocessing step, a *smoothing spline curve-fitting* method was applied to the raw data acquired from the OptiTrack system. The MATLAB® *fit* function was used in this step with the smoothing parameter $p = 0.998$ and option *Normalize = on*.

Model Verification and Validation

Model Verification

The verification step involves ensuring that the model is correctly implemented and functions as intended. This was achieved by simulating the model with known expected outputs.

Verification was conducted using known kinematic data to generate time-varying torque signals via the Euler-Lagrange formulation (see section "Dynamic Modeling").

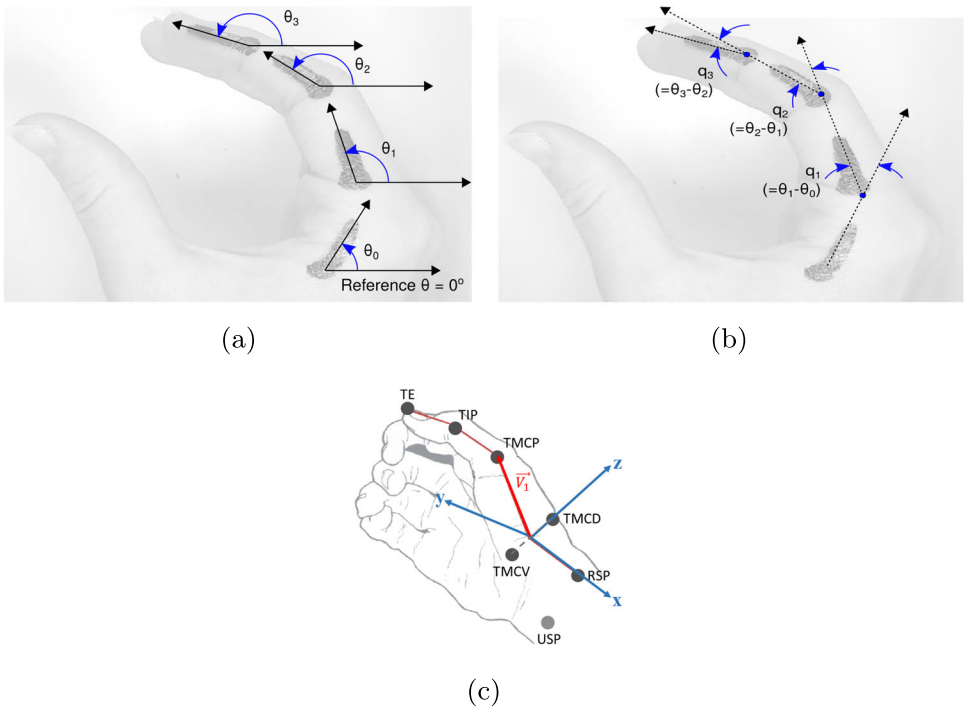

Fig. 6 Obtaining the joint position configurations. a) Illustration of the joint angular position of the digit segments relative to the horizontal; b) Joint configurations calculated by the difference between the angular position of the consecutive segments. c) Direction vector $\vec{V}_1$, which is the movement direction of the first metacarpal segment [1]

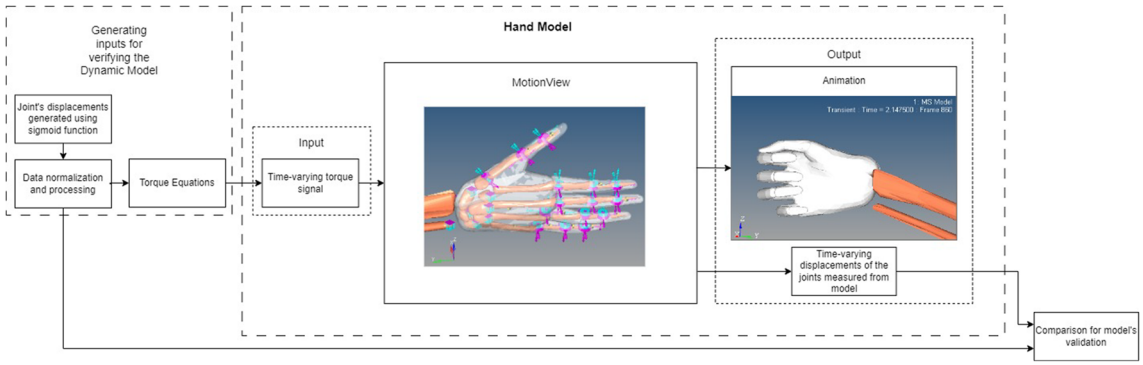

Fig. 7 Block diagram illustrating the verification process

These torque signals were then used as inputs to the model. By applying these torques, the hand segments moved according to the model's dynamics, thereby reducing the joint kinematic data outputs. These outputs were compared with the kinematic data used to generate the torques, as illustrated in Fig. 7.

For the verification process, the kinematic data were generated using a sigmoid function, equation (9), with horizontal beginning and end segments. The signal was defined by the following parameters: amplitude $a\_sigm = 1.2$, steepness $b\_sigm = 1$, and x-axis shift $c\_sigm = 5$. The time vector consisted of 4300 points distributed over 10.37 *seconds*. To ensure horizontal segments at the beginning and end, two lines with values of 0 and 1 (150 points each) were appended to the start and end of the signal, with the sigmoid function in the middle. A smoothing spline with a smoothing parameter of 0.99 was applied to the entire signal to ensure a smooth transition between segments. The resulting signal was then normalized to generate the torques' inputs for each joint: Q_1, Q_2, and Q_3 for the thumb, and q_1, q_2, and q_3 for the other digits, as specified in section "Inputs of the torque equations".

$$\sigma = a\_sigm \cdot \frac{1}{1 + e^{-b\_sigm \cdot (time - c\_sigm)}} \tag{9}$$

Model validation

The aim of validating the computational model was to assess its functionality with a limited dataset acquired from six participants as a pilot test.

In this study, the computational model was validated by comparing its outputs against experimentally obtained kinematic data. The validation process involved estimating time-varying torque signals through torque equations, derived from the Euler-Lagrange formulation, Section "Dynamic Modeling". The experimental joint displacement data were used as inputs for the torque equations. These estimated torque signals were used as inputs to the multibody model. As a consequence of applying these torques, the hand segments moved according to the model's dynamics. The model outputs the joint displacements, measured during the simulated movement induced by these torques. The model's outputs were subsequently compared with the participants' kinematic

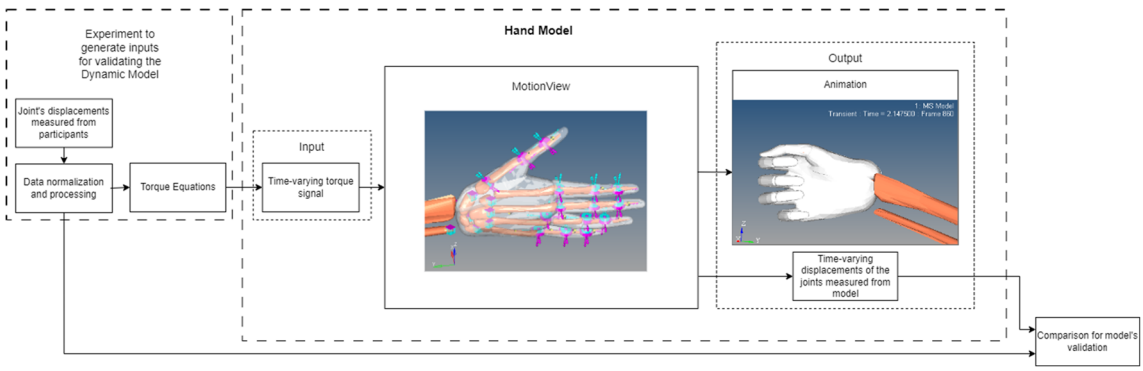

Fig. 8 Block diagram illustrating the validation process

data (expected outputs) to assess the model's accuracy. The block diagram (Fig. 8) illustrates this process. In total, the validation was performed in three ways, which are further described below.

1. **Analysis of the obtained kinematic output dataset**: The model's kinematic output dataset, which includes the configuration's displacements, was analyzed in contrast to the joint kinematics data acquired from the subjects. The coefficient of correlation was chosen to evaluate the pairs of expected (kinematic data measured from participants) and obtained (model kinematic outputs) datasets, as illustrated by the block diagram (Fig. 8).
2. **Evaluation of the physiology of the pinching motion:** The fidelity of the resulting pinching posture was assessed in contrast to its expected physiological characteristics. This involved a visual inspection of the animations to ensure that the posture obtained during the animation and the final pinch posture aligned with the expected physiological patterns.
3. **Comparison to literature data:** The position of the trapeziometacarpal joint in the model was compared to the data available in the literature [1, 3, 4, 23].

Results and Discussion

The present study consists of developing a computational model of the human hand describing the physiology of lateral pinch movement. The model enables the evaluation of the pinch movement and the resulting pinch posture of individuals, regardless of their age or the size of hand segments. The model was developed to analyze only lateral pinch movement. For other types of movement, the model should be adapted. This section presents the results obtained from the verification and validation approaches, which are described in subsection "Model Verification".

Model Verification

Figure 9 displays the generated sigmoid curves used for model verification. Panel (a) shows the joint displacements for the thumb, and panel (b) shows those for the other digits.

The pinch posture obtained from the simulation, depicted in Fig. 10, demonstrates that the hand segments achieved a realistic lateral pinch posture, consistent with expected physiological characteristics.

Table 2 presents the results of the model verification. The table compares the expected (generated sigmoid signals) and obtained (simulated model outputs) joint displacements in terms of the correlation coefficient and percentage difference. The maximum percentage difference observed was 7.21%, with a mean of 1.90%. The correlation coefficients ranged from 0.9976 to 1, indicating a high level of fidelity in the model's performance.

Furthermore, Fig. 12 in Appendix B illustrates the comparison between the expected and obtained joint displacements, demonstrating that the model outputs closely follow the expected signals.

The minimal differences between the expected and obtained results fall within acceptable ranges and can be attributed to several factors. One primary reason is the simplified implementation of the model, which includes approximating hand segments as cylinders for calculating the moments of inertia. Additionally, the numerical errors inherent in the simulation process contribute to these discrep-

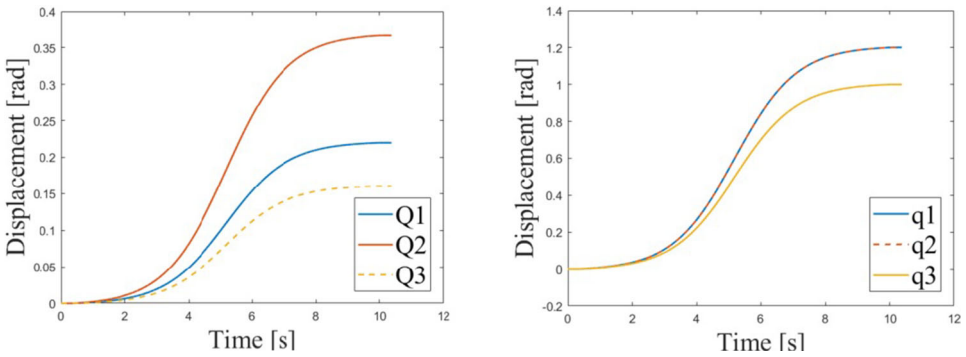

Fig. 9 Sigmoid curves generated for model verification. a) Generated Q1, Q2 and Q3 joint displacements of the thumb. b) Generated q1, q2 and q3 joint displacements for the other digits

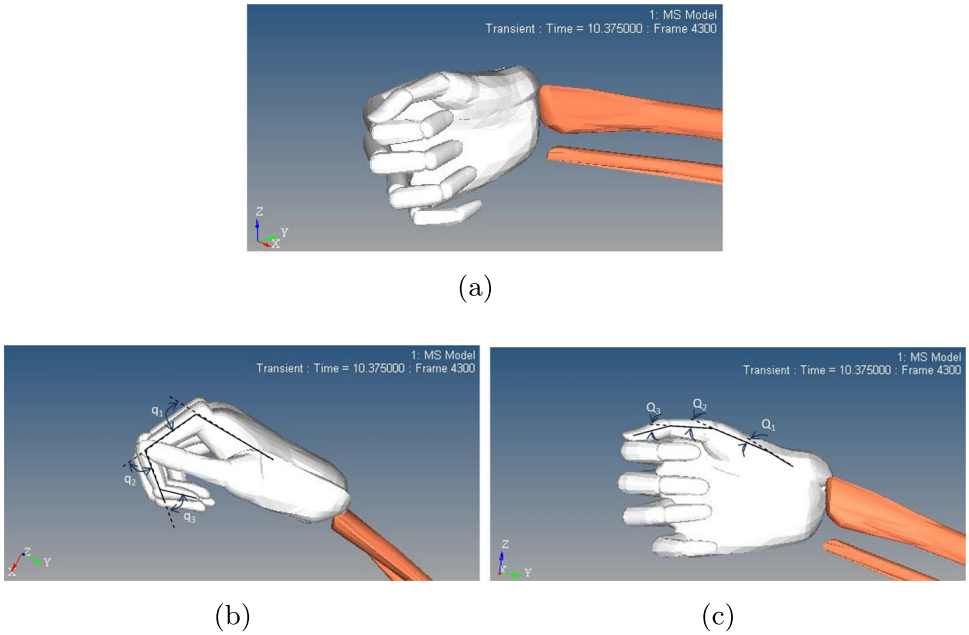

Fig. 10 Pinch posture obtained from the animation generated by simulating the computational model with torque signals estimated by sigmoid signals (a), overlayed by an illustration marking the hand segments and position configuration of b) index joints (q_1, q_2, and q_3) and c) thumb joints (Q_1, Q_2, and Q_3)

ancies. Despite these simplifications, the model demonstrates a high level of accuracy and robustness in replicating the kinematic behavior. These results confirm the model's correct implementation and functionality, as evidenced by the high correlation coefficients and low percentage differences between the expected and obtained joint displacements. This validates the model's ability to simulate the complex dynamics of hand movements with a high degree of precision.

Table 2 Results of model verification with the torque signals estimated with the generated sigmoid signals

Digit	Configuration	Difference final position (%)	Correlation coeficient
Thumb	Q_1	7.211	1.000
	Q_2	3.503	0.9997
	Q_3	3.7976	0.9976
Index	q_1	0.6137	1.0000
	q_2	1.5724	1.0000
	q_3	2.0581	0.9999
Middle	q_1	0.1521	1.0000
	q_2	0.5421	1.0000
	q_3	2.3339	0.9998
Ring	q_1	0.0727	1.0000
	q_2	1.3674	1.0000
	q_3	3.35	0.9997
Small	q_1	0.1522	1.0000
	q_2	0.3025	1.0000
	q_3	1.6206	0.9999

Expected (generated sigmoid signals), Fig. 9, and data obtained from the model's simulation are compared in terms of correlation coefficient (r) and percentage difference (*difference (%)*) between the endpoints of the corresponding expected and obtained datasets

Table 3 Results of model validation with the torque signals estimated by data acquired from subjects 1 to 6

Subject							
1	Digit:	Index			Thumb		
	Configuration	q_1	q_2	q_3	Q_1	Q_2	Q_3
	Difference (%)	0.5992	0.0307	1.8138	12.7186	1.4880	12.6905
	r	0.9650	0.9670	0.9647	0.9996	0.9987	0.9931
2	Digit:	Index			Thumb		
	Configuration	q_1	q_2	q_3	Q_1	Q_2	Q_3
	Difference (%)	1.8248	3.9187	0.9914	16.8264	3.4088	22.6624
	r	0.9999	0.9998	0.9999	0.9995	0.9951	0.9804
3	Digit:	Index			Thumb		
	Configuration	q_1	q_2	q_3	Q_1	Q_2	Q_3
	Difference (%)	1.6849	3.1686	0.7926	10.7015	4.3138	5.0165
	r	1.0000	0.9999	1.0000	0.9999	0.9998	0.9967
4	Digit:	Index			Thumb		
	Configuration	q_1	q_2	q_3	Q_1	Q_2	Q_3
	Difference (%)	0.8713	1.8299	0.8929	8.6112	6.4777	2.3556
	r	1.0000	0.9999	1.0000	1.0000	0.9999	0.9988
5	Digit:	Index			Thumb		
	Configuration	q_1	q_2	q_3	Q_1	Q_2	Q_3
	Difference (%)	20.4494	5.8023	7.4119	18.6724	4.2222	0.1286
	r	0.9971	0.9893	0.9983	0.9996	0.9999	0.9978
6	Digit:	Index			Thumb		
	Configuration	q_1	q_2	q_3	Q_1	Q_2	Q_3
	Difference (%)	2.7178	3.5164	1.8180	10.2995	2.3802	14.9560
	r	1.0000	0.9998	1.0000	0.9999	0.9982	0.9896

The expected (experimental) and obtained (simulated) data from the model were compared in terms of the correlation coefficient (r) and percentage difference (*difference (%)*) between the endpoints of the corresponding expected and obtained datasets

Model Validation

The angular displacement over time of the configurations was acquired from six subjects during the experiment described in section "Experimental Analysis". These data were used as inputs to the torque equations, and the torque signals were applied to the simulations. The torques generated the movement of hand segments according to the model's dynamics. The time-varying displacements of the joints were output by the model. Appendix C presents the plots of the expected (experimental joint displacements) and obtained (model joint displacements) displacements for each subject. Figures 13 and 14 show plots of the configurations of the index finger and thumb of the participants.

The correlation coefficient (r) between the experimental joint displacement and the model's output datasets was used to evaluate the system functionality. The estimated coefficients are displayed in Table 3. The highest and lowest correlation coefficients obtained are 1.0000 and 0.9647, respectively.

The computation times for each of the six simulations are detailed in Table 4. The total elapsed time includes the processing, core analysis, and postprocessing/messaging durations.

Table 4 Q_1 configuration measured from the simulations in the pinch posture for each of the six simulations related to participants 1 to 6; and computation time information, which consists of the summation of processing time, core analysis, and postprocessing/messaging

Subject	1	2	3	4	5	6
Total elapse time [s]	1.201	1.264	1.107	1.170	1.263	1.342
Q_1 in pinch posture [rad]	0.2501	0.2560	0.2436	0.2395	0.2614	0.2429

To assess the functionality of the model concerning pinch posture, the endpoints of the expected and obtained displacement datasets were analyzed for their percentage difference, as detailed in Table 3. The analysis revealed the highest and lowest percentage differences to be 22.66% and 0.03%, respectively, with an average difference of 6.06% between the expected and obtained joint angular displacements.

The lateral pinch posture was also assessed in terms of the physiological pattern resulting from the simulations. Figure 11 presents the pinch posture obtained from the animation generated by simulating the computational model using torque signal data estimated by subject 3 kinematic data. The resulting posture was overlayed by an illustration marking the hand segments and configuration of the index joints, q_1, q_2, and q_3, and thumb joints, Q_1, Q_2, and Q_3, as shown in Fig. 11(b) and (c).

For a comprehensive view of the obtained pinch posture from the six simulations, please refer to Appendix D, specifically Fig. 15. Furthermore, the adduction/abduction positions of the TMCJ in the Q_1 configuration were measured during simulations in the pinch posture, and the results are detailed in Table 4.

The model's main advantage is its ability to facilitate the study of hand movements in a computational environment, as indicated by the analysis of kinematic and dynamic variables estimated by the simulation solver, which has a notably low computational cost, with the maximum observed computation time being 1.342 *s* for simulation with torque signals estimated by using kinematic data from subject 6 (Table 4). Additionally, the model's simulation provides animated representations of the movement, which assists in the identification of potential pathologies. The efficiency of the dynamic model in terms of computational resources also makes it a strong candidate for serving as the foundation for designing prosthetic and orthosis solutions.

While direct imaging of the trapeziometacarpal joint position (e.g., through tomography or radiography) can offer precise positioning, the present study adopts the validated kinematic approximation described by Barroso [1, 3, 23]. This method provides a reliable approximation of joint movement with minimal positioning error, thus making it suitable for our analysis without subjecting volunteers to radiation exposure.

The model was validated through three approaches. The initial validation method involved a comparison between the achieved joint position configurations (measured from the model simulation) and the expected configurations (experimentally acquired from subjects), examining both their angular displacements over time and their final positions in the pinch posture. The second approach focused on assess-

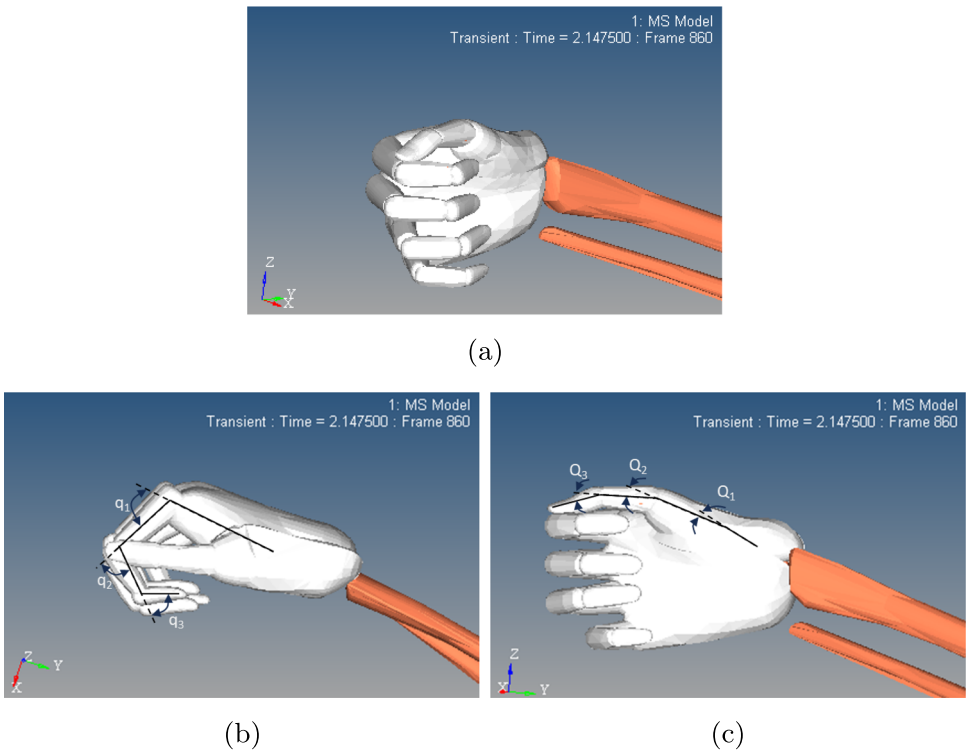

Fig. 11 Pinch posture obtained from the animation generated by simulating the computational model using torque signal data estimated by subject 3 kinematic data (a), overlayed by an illustration marking the hand segments and position configuration of b) index joints (q_1, q_2, and q_3) and c) thumb joints (Q_1, Q_2, and Q_3)

ing the fidelity of the resulting pinch posture in contrast to its expected physiological characteristics. Finally, the validation was further reinforced by aligning the angular position of the TMCJ in the pinching posture with the literature findings.

The first validation approach consisted of a pilot test to validate the functionality of the system by providing data acquired from a limited set of participants. Although direct force measurements can enhance the validation process, direct measurement of torques would require highly invasive procedures, potentially compromising natural movement. Hence, kinematic measurements were employed as a less invasive alternative. The goal was not to validate the model with a high number of subjects but rather to demonstrate the model's functionality.

The major limitation of the validation system lies in the necessary infrastructure for capturing the 3D positions of the subjects' joints. The acquired joint displacements are used as inputs to the torque equations for estimating torque signals which are inputs to the model. During the experiments, the proximity of the reflexive markers induced the OptiTrack system to close its positions, introducing systematic errors into the acquired data. The minimum size of the hand segment was established to be 18.0 *mm* to minimize measurement errors. Additionally, the consistency of the joint positions was checked in relation to the 3D plot, with manual corrections when applicable and possible. Finally, the curve fitting processing method attenuated considerable inconsistencies in the raw data.

The processed acquired data are presented in the Appendix C for each subject's index finger (Fig. 13) and thumb (Fig. 14), labeled as *expected* signals. The plots display pairs of expected (experimentally acquired from subjects) and obtained (output of the model) signals. The plots in Fig. 13(d) depict a more accurate representation of the expected joint displacement patterns during the pinching motion. The lower-frequency components observed in the remaining plots and overshoot occurrences can be attributed to measurement errors.

The inconsistent spectral components of the displacements, with frequencies approximately equal to 1 Hz, result in torques that are slightly incompatible with the system's dynamic. Consequently, these torques lead to minor errors in trajectory tracking, even in the transient state, as in the steady state values performed in the pinching posture. These differences are presented in Table 3.

Despite the presence of measurement errors, the average disparity between the expected and obtained joint angular displacements was found to be 6.06%, indicating a high level of fidelity in the model's performance and falling within the anticipated range of results. Furthermore, upon visual inspection, it becomes evident that the obtained data closely align with the expected values. According to the correlation analysis between pairs of obtained and expected configuration data, a minimum correlation coefficient of 0.9647 was observed, indicating a strong positive linear relationship and a robust correlation [24].

It is essential to note that the participants' data were not utilized for calibration or parameterization of the model, but were used exclusively for validation purposes. This approach ensures that the model is validated independently of the experimental data, thereby avoiding any circular logic in the model.

Furthermore, the validation process was designed to test the accuracy and reliability of the model as a whole. Although the participant data are used to derive the input torques, the resulting movement in the model depends on the comprehensive biomechanical and physical principles embedded in the model, not just on the torques. Thus, the model's ability to reproduce the experimentally observed kinematics validates its underlying structure and parameters, independent of the initial derivation of the input torques.

The pinch postures rendered in the animations generated by simulating the model with torques estimated by the kinematic data acquired from all six subjects, Fig. 4(b), were evaluated via visual inspection. The postures are consistent with the expected physiological patterns according to the available literature [1, 3, 4, 23, 25].

The range of the adduction/abduction position of the TMCJ in the lateral pinch posture of asymptomatic individuals measured by Barroso [1, 3, 23] is $Q_1 = 0.1780 \pm 0.0785$ rad. However, Leon [4] defined the possible ranges of rotation of the TMCJ in the adduction/abduction direction within the ranges -0.5236 and 1.0472 *rad* for general hand movements. As presented in Table 4, all simulations fell within the limits defined by Leon. Moreover, except for using data from subject 5, all simulations exhibited Q_1 configurations that fell within the limits defined by Barroso. The Q_1 angular position obtained from simulation 5 slightly exceeded Barroso's maximum limit by 1.9%, this discrepancy is within the expected range of results and is attributed to measurement and numerical errors inherent in the simulation process.

Model Limitations

Despite the robustness and accuracy demonstrated by our biomechanical hand model, several limitations should be acknowledged:

1. **2D Movements Analysis:** Our study only analyzed 2D movements, although the model is designed to support 3D movements. Future work should extend the validation to 3D movements to fully leverage the model's capabilities and improve its applicability.

2. **Single Pinch Posture:** The current study covers only one type of pinch posture. Expanding the range of analyzed movements would provide a more comprehensive validation. However, our model is designed to be easily adaptable for different types of hand movements.
3. **Absence of Dissipative Components:** The model does not include dissipative components, such as friction and damping. Incorporating these elements could enhance the model's realism and fidelity to real-world dynamics.
4. **Rigid Body Assumption:** The hand segments are modeled as rigid bodies. Implementing flexible body dynamics could further improve the model accuracy. Nonetheless, the rigid body assumption contributes to the model's low computational cost, which is advantageous for various practical applications.

Conclusions

In conclusion, this study developed a versatile computational model of a human hand to simulate lateral pinch movement, enabling efficient analysis of kinematic and dynamic variables with minimal computational cost. The model aids pathology identification through animated movement representations and holds promise for designing prosthetic and orthotic solutions. Although designed for lateral pinch analysis, it can be adapted for other hand movements.

The average disparity between the expected and obtained joint angular displacements was 6.06 % and 1.90 % during validation and verification stages, suggesting high fidelity in the model performance

Validation through three approaches and model verification confirmed the model's functionality and accuracy, with an average joint angular displacement difference of 6.06 % and 1.90 % between expected and obtained values during validation and verification stages. Visual and correlation analyses demonstrated its robustness, producing pinch postures closely matching physiological patterns despite minor measurement discrepancies.

This model offers significant potential for advancing hand movement studies and designing rehabilitation solutions, and remains a valuable tool for hand biomechanics research despite data acquisition challenges.

Model Availability

The biomechanical model simulation files developed and used in this research are publicly available on GitHub at the following link: https://github.com/alinedefarial/Biomechanical_Model_MotionView/tree/main. This repository includes all the files necessary to replicate the simulations and analyses presented in this manuscript.

A Derived Torque Equations

This appendix provides the torque equations for estimating time-varying torques through joint kinematic data derived by solving equation (2) with reference to equations (3) to (8), as discussed in section "Dynamic Modeling". These resulting torque equations are expressed in equations (10) to (12).

$$\begin{aligned}\tau_1 = {} & (2 \cdot D_1 \cdot (M_3 \cdot D_{cm3} \cdot \cos(q_3) + D_2 \cdot M_3 + D_{cm2} \cdot M_2) \cdot \cos(q_2) + \\ & -2 \cdot \sin(q_2) \cdot \sin(q_3) \cdot D_1 \cdot M_3 \cdot D_{cm3} + 2 \cdot \cos(q_3) \cdot D_2 \cdot M_3 \cdot D_{cm3} + \\ & + (D_{cm3}^2 + D_1^2 + D_2^2) \cdot M_3 + D_{cm1}^2 \cdot M_1 + M_2 \cdot D_{cm2}^2 + D_1^2 \cdot M_2 + I_1 + \\ & + I_2 + I_3) \cdot \ddot{q_1} + (D_1 \cdot (M_3 \cdot D_{cm3} \cdot \cos(q_3) + D_2 \cdot M_3 + \\ & + D_{cm2} \cdot M_2) \cdot \cos(q_2) - \sin(q_2) \cdot \sin(q_3) \cdot D_1 \cdot M_3 \cdot D_{cm3} + \\ & + 2 \cdot \cos(q_3) \cdot D_2 \cdot M_3 \cdot D_{cm3} + (D_{cm3}^2 + D_2^2) \cdot M_3 + M_2 \cdot D_{cm2}^2 + I_2 + \\ & + I_3) \cdot \ddot{q_2} + (M_3 \cdot D_{cm3} \cdot \cos(q_3) \cdot \cos(q_2) \cdot D_1 + \\ & + \cos(q_3) \cdot D_2 \cdot M_3 \cdot D_{cm3} - \sin(q_2) \cdot \sin(q_3) \cdot D_1 \cdot M_3 \cdot D_{cm3} + \\ & + M_3 \cdot D_{cm3}^2 + I_3) \cdot \ddot{q_3} - (M_3 \cdot D_{cm3} \cdot \cos(q_2) \cdot \sin(q_3) + \\ & + \sin(q_2) \cdot (M_3 \cdot D_{cm3} \cdot \cos(q_3) + D_2 \cdot M_3 + D_{cm2} \cdot M_2)) \cdot D_1 \cdot \dot{q_2}^2 + \\ & + (-2 \cdot M_3 \cdot D_{cm3} \cdot (\cos(q_2) \cdot \sin(q_3) \cdot D_1 + \cos(q_3) \cdot \sin(q_2) \cdot D_1 + \\ & + \sin(q_3) \cdot D_2) \cdot \dot{q_3} - 2 \cdot \dot{q_1} \cdot (M_3 \cdot D_{cm3} \cdot \cos(q_2) \cdot \sin(q_3) + \\ & + \sin(q_2) \cdot (M_3 \cdot D_{cm3} \cdot \cos(q_3) + D_2 \cdot M_3 + D_{cm2} \cdot M_2)) \cdot D_1) \cdot \dot{q_2} + \\ & - M_3 \cdot D_{cm3} \cdot (\cos(q_2) \cdot \sin(q_3) \cdot D_1 + \cos(q_3) \cdot \sin(q_2) \cdot D_1 + \\ & + \sin(q_3) \cdot D_2) \cdot \dot{q_3}^2 - 2 \cdot M_3 \cdot D_{cm3} \cdot \dot{q_1} \cdot (\cos(q_2) \cdot \sin(q_3) \cdot D_1 + \\ & + \cos(q_3) \cdot \sin(q_2) \cdot D_1 + \sin(q_3) \cdot D_2) \cdot \dot{q_3} + \\ & + (M_3 \cdot D_{cm3} \cdot \cos(q_1) \cdot \cos(q_3) - M_3 \cdot D_{cm3} \cdot \sin(q_1) \cdot \sin(q_3) + \\ & + \cos(q_1) \cdot (D_{cm2} \cdot M_2 + D_2 \cdot M_3)) \cdot g \cdot \cos(q_2) - \\ & + g \cdot (M_3 \cdot D_{cm3} \cdot \sin(q_1) \cdot \cos(q_3) + M_3 \cdot D_{cm3} \cdot \cos(q_1) \cdot \sin(q_3) + \\ & + \sin(q_1) \cdot (D_{cm2} \cdot M_2 + D_2 \cdot M_3)) \cdot \sin(q_2) + g \cdot (D_{cm1} \cdot M_1 + \\ & + D_1 \cdot M_2 + D_1 \cdot M_3) \cdot \cos(q_1) \end{aligned} \tag{10}$$

$$\begin{aligned}\tau_2 = {} & (D_1 \cdot (M_3 \cdot D_{cm3} \cdot \cos(q_3) + M_3 \cdot D_2 + D_{cm2} \cdot M_2) \cdot \cos(q_2) + \\ & - \sin(q_2) \cdot \sin(q_3) \cdot D_1 \cdot M_3 \cdot D_{cm3} + 2 \cdot \cos(q_3) \cdot D_2 \cdot M_3 \cdot D_{cm3} + \\ & + (D_{cm3}^2 + D_2^2) \cdot M_3 + M_2 \cdot D_{cm2}^2 + I_2 + I_3) \cdot \ddot{q_1} + \\ & + (2 \cdot \cos(q_3) \cdot D_2 \cdot M_3 \cdot D_{cm3} + (D_{cm3}^2 + D_2^2) \cdot M_3 + M_2 \cdot D_{cm2}^2 + I_2 + \\ & + I_3) \cdot \ddot{q_2} + \ddot{q_3} \cdot (\cos(q_3) \cdot D_2 \cdot M_3 \cdot D_{cm3} + M_3 \cdot D_{cm3}^2 + I_3) + \\ & + D_1 \cdot (M_3 \cdot D_{cm3} \cdot \cos(q_2) \cdot \sin(q_3) + \sin(q_2) \cdot (M_3 . D_{cm3} \cdot \cos(q_3) + \\ & + M_3 \cdot D_2 + D_{cm2} \cdot M_2)) \cdot \dot{q_1}^2 - 2 \cdot \dot{q_1} \cdot M_3 \cdot D_{cm3} \cdot \dot{q_3} \cdot \sin(q_3) \cdot D_2 + \\ & - M_3 \cdot D_{cm3} \cdot \dot{q_3}^2 \cdot \sin(q_3) \cdot D_2 - 2 \cdot \dot{q_2} \cdot M_3 \cdot D_{cm3} \cdot \dot{q_3} \cdot \sin(q_3) \cdot D_2 + \\ & + (M_3 \cdot D_{cm3} \cdot \cos(q_1) \cdot \cos(q_3) - M_3 \cdot D_{cm3} \cdot \sin(q_1) \cdot \sin(q_3) + \\ & + \cos(q_1) \cdot (D_{cm2} \cdot M_2 + D_2 \cdot M_3)) \cdot g \cdot \cos(q_2) - \\ & + g \cdot (M_3 \cdot D_{cm3} \cdot \sin(q_1) \cdot \cos(q_3) + M_3 \cdot D_{cm3} \cdot \cos(q_1) \cdot \sin(q_3) + \\ & + \sin(q_1) \cdot (D_{cm2} \cdot M_2 + D_2 \cdot M_3)) \cdot \sin(q_2) \end{aligned} \tag{11}$$

$$\begin{aligned}\tau_3 = {} & (M_3 \cdot D_{cm3} \cdot (\cos(q_2) \cdot D_1 + D_2) \cdot \cos(q_3) + \\ & - \sin(q_2) \cdot \sin(q_3) \cdot D_1 \cdot M_3 \cdot D_{cm3} + M_3 \cdot D_{cm3}^2 + I_3) \cdot \ddot{q_1} + \end{aligned}$$

$$
\begin{aligned}
&+ (\cos(q_3) \cdot D_2 \cdot M_3 \cdot D_{cm3} + M_3 \cdot D_{cm3}^2 + I_3) \cdot \ddot{q}_2 + \\
&+ \ddot{q}_3 \cdot (D_{cm3}^2 \cdot M_3 + I_3) + D_{cm3} \cdot ((\cos(q_2) \cdot D_1 + D_2) \cdot \sin(q_3) + \\
&+ \cos(q_3) \cdot \sin(q_2) \cdot D_1) \cdot M_3 \cdot \dot{q}_1{}^2 + \\
&+ 2 \cdot \dot{q}_1 \cdot \dot{q}_2 \cdot M_3 \cdot D_{cm3} \cdot \sin(q_3) \cdot D_2 + \sin(q_3) \cdot D_2 \cdot M_3 \cdot D_{cm3} \cdot \dot{q}_2{}^2 + \\
&- g \cdot M_3 \cdot D_{cm3} \cdot (\cos(q_1) \cdot \sin(q_2) + \sin(q_1) \cdot \cos(q_2)) \cdot \sin(q_3) + \\
&+ g \cdot M_3 \cdot D_{cm3} \cdot (\cos(q_1) \cdot \cos(q_2) - \sin(q_1) \cdot \sin(q_2)) \cdot \cos(q_3) \qquad (12)
\end{aligned}
$$

B Results of Model Verification

Figure 12 illustrates the comparison between the expected joint displacements, generated using sigmoid functions, and the joint displacements obtained from the model simulation. This comparison is crucial for validating the model's accuracy in replicating realistic joint movements.

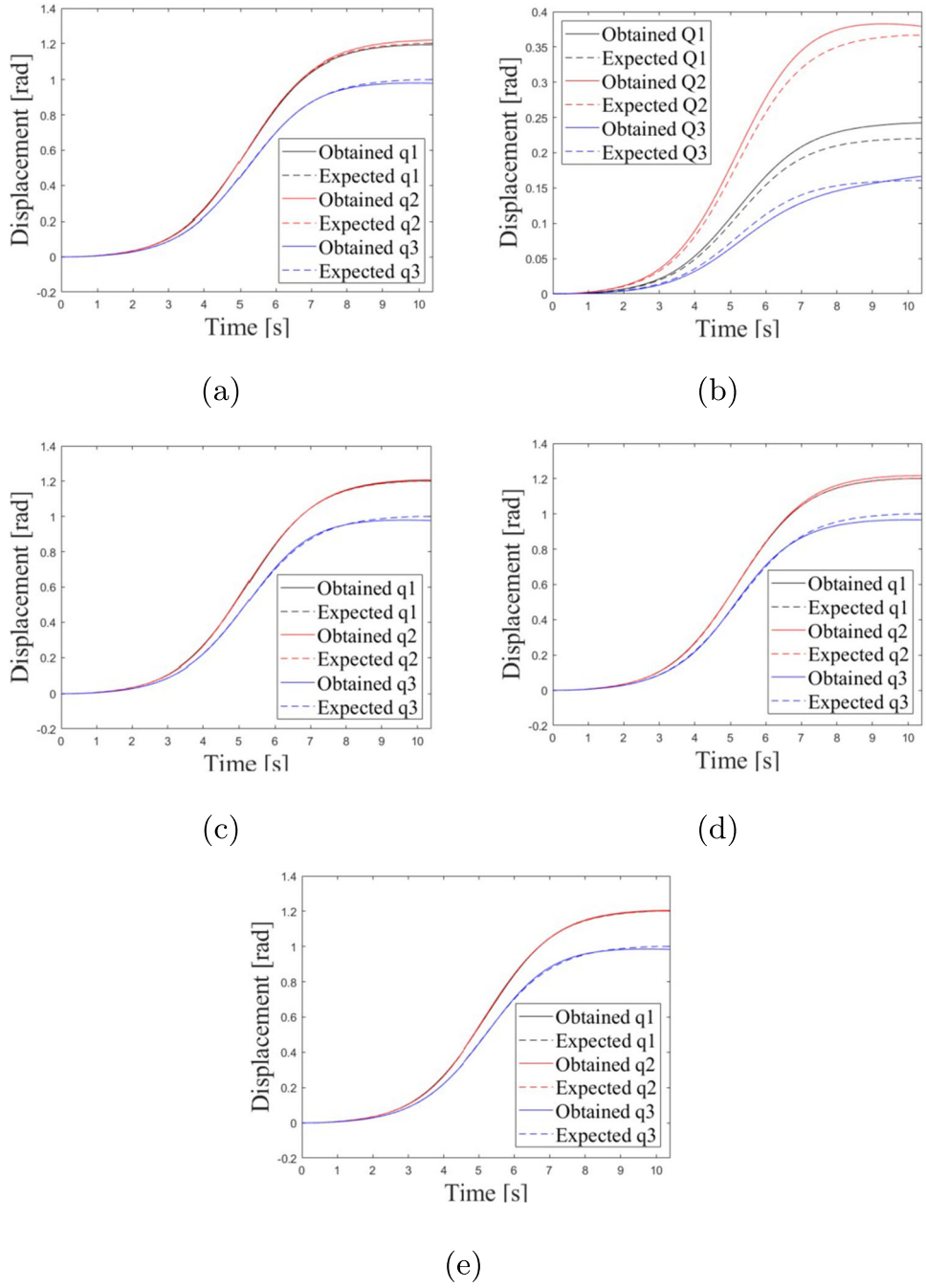

Fig. 12 Plots of the expected joint displacements, generated using sigmoid functions, compared with the obtained joint displacements from the model's simulation. a) Index, b) thumb, c) middle, d) ring, e) small digit.)

The expected joint displacements were created using the parameters detailed in the verification section, resulting in smooth, time-varying signals that served as input torques for the model. The model's outputs, representing the actual joint movements, were then plotted against these expected signals.

1. **Thumb Joints** (Q_1, Q_2 **and** Q_3): The model outputs for the thumb joints closely follow the expected signals, as shown in panel (a). The slight deviations observed at certain points are minimal and fall within an acceptable range, confirming the model's ability to accurately simulate thumb movements.
2. **Index and Other Digits Joints** (q_1, q_2 **and** q_3): Similar to the thumb joints, the outputs for the index and other digits also exhibit high fidelity to the expected signals, as illustrated in panel (b). The correlation coefficients and percentage differences, detailed in Table 2, further substantiate this observation.

C Results of Digit Displacement for each Subject

This appendix includes plots illustrating the displacement over time for both the expected (experimentally acquired from subjects) and obtained (output of model's simulations) configurations of each subject. The dataset comprises data acquired from all six participants, which serve for estimating the torque signals, which are the input of the model, and the corresponding output from the model's simulations. Figures 13 and 14 display the configurations of the index finger and thumb for each participant.

D Pinch Posture Obtained for each Subject

The present appendix displays the obtained pinch postures resulting from simulations with torque signals estimated by kinematic data experimentally acquired from subjects 1 to 6, as illustrated in Fig. 15.

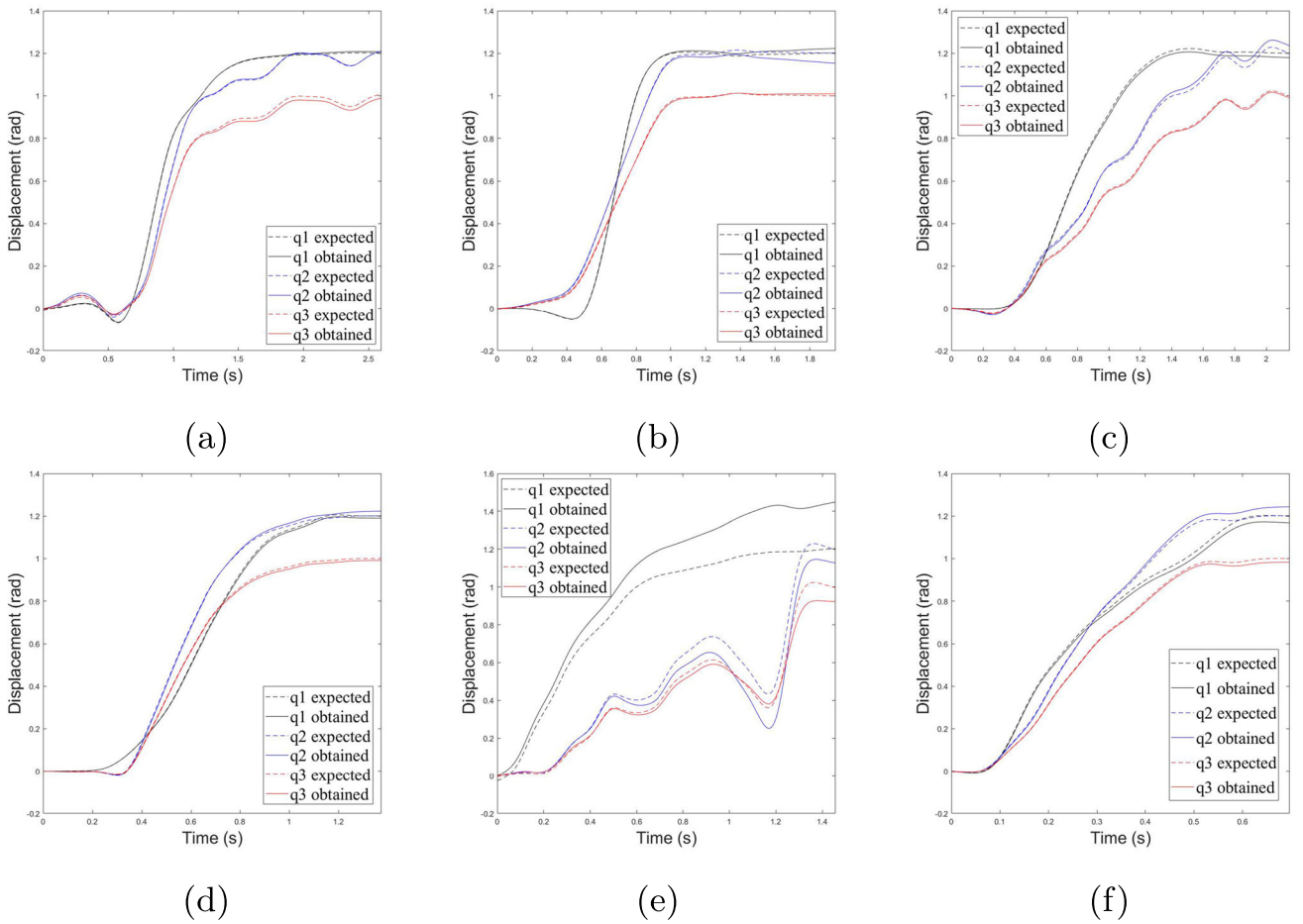

Fig. 13 Plots of the joint displacement of the index finger in the expected (experimentally acquired from subjects) and obtained (measured from the model simulation) configurations over time for subjects 1 (*a*) to 6 (*f*)

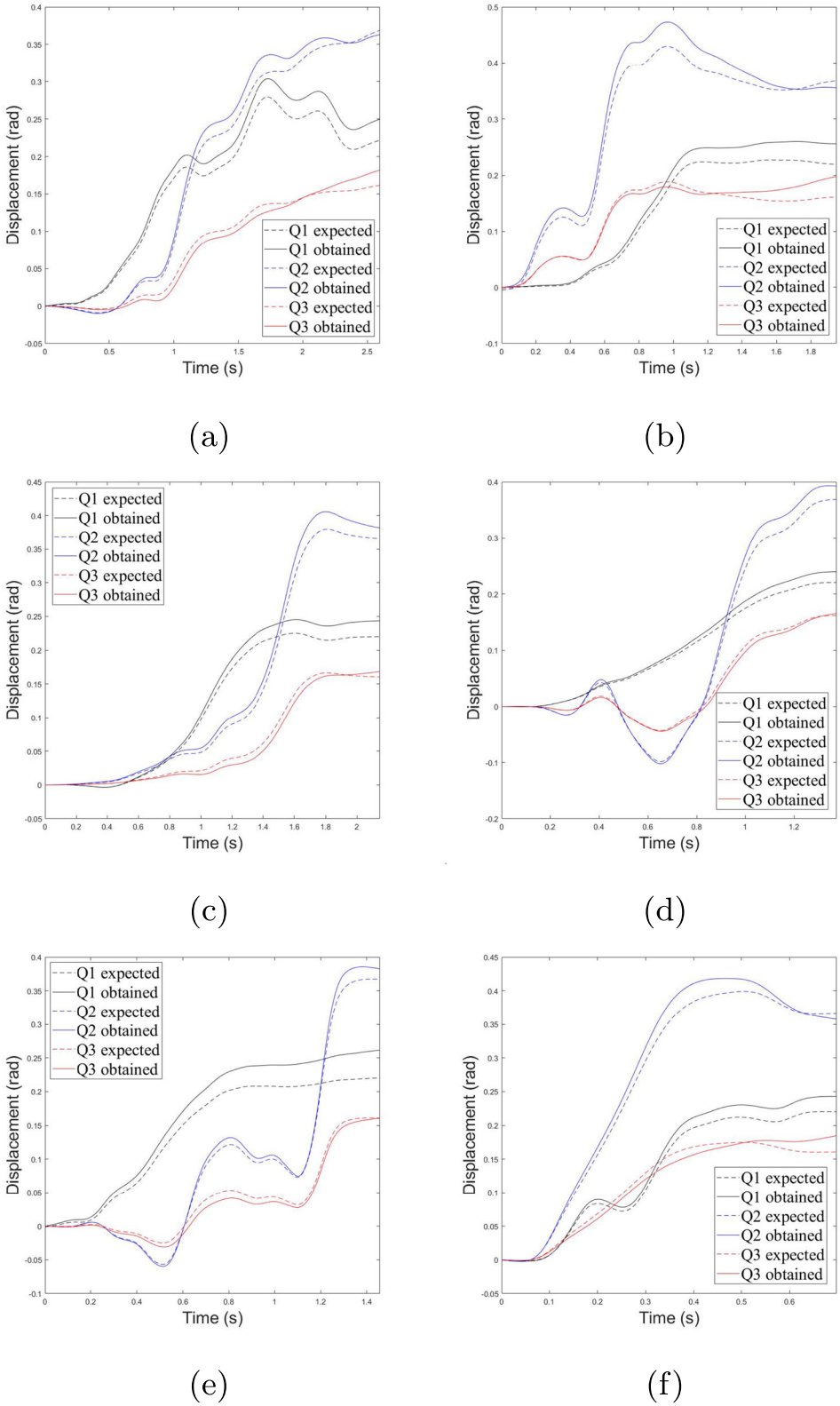

Fig. 14 Plots of the displacement of the thumb in the expected (experimentally acquired from subjects) and obtained (measured from the model simulation) configurations over time for subjects 1*a*-6*f*

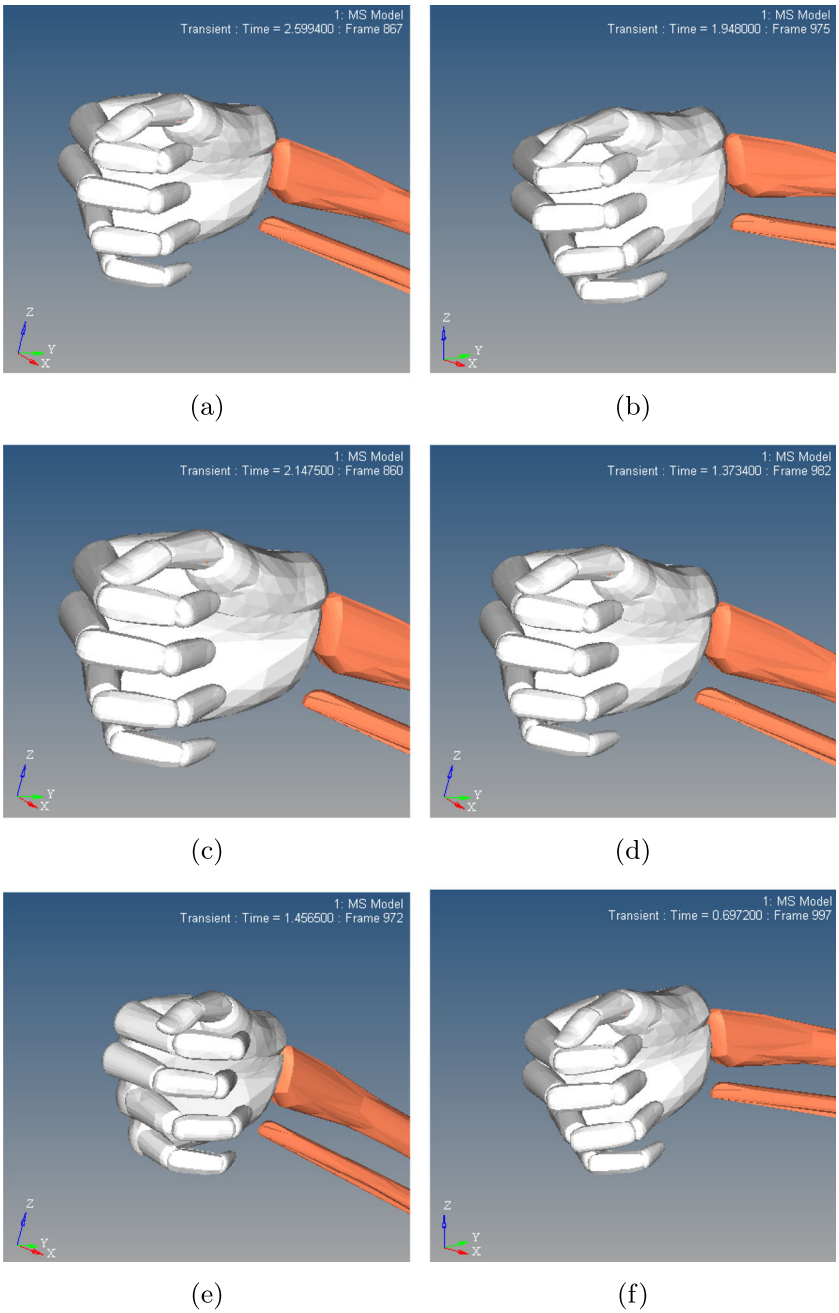

Fig. 15 Pinch posture obtained from the animation generated by simulating the computational model with torque signals estimated from kinematic data experimentally acquired from subjects a) 1; b) 2; c) 3; d) 4; e) 5; and f) 6

Acknowledgements This study was financed in part by the Coordenação de Aperfeiçoamento de Pessoal de Nível Superior - Brasil (CAPES) - Finance Code 001
The authors thank the BME MOGI MotionLab team for providing access and support during the experiments to acquire the mechanical configurations of the subjects using the OptiTrack system.
Project no. TKP-6-6/PALY-2021 has been implemented with support provided by the Ministry of Culture and Innovation of Hungary from the National Research, Development and Innovation Fund, financed under the TKP2021-NVA funding scheme.

Funding Open access funding provided by Budapest University of Technology and Economics.

Declarations

Conflicts of Interest Statement The authors have no conflicts of interest to declare.

References

1. Barroso PN (2007) Análise da Variação Angular Funcional da Articulação Trapeziometacarpiana. Federal University of Minas Gerais, Minas Gerais, Brazil
2. Lancet T (1954) Surgery of the hand. The Lancet, pp 67–68
3. Barroso PN (2010) Nova Órtese de Extensão de Punho e Abdutora de Polegar para Crianças com Paralisia Cerebral: Avaliação de suas Contribuições para o Incremento da Funcionalidade Manual. Federal University of Minas Gerais
4. Léon B, Morales A, Sancho-Bru J (2013) 5, The model of the human hand. In: From robot to human grasping simulation. Springer, pp 123–174
5. Liu Y, Jiang L, Liu H, Ming D (2021) A systematic analysis of hand movement functionality: qualitative classification and quantitative investigation of hand grasp behavior. Front Neurorobot 15:658075
6. Buchholz B, Armstrong TJ (1992) A kinematic model of the human hand to evaluate its prehensile capabilities. J Biomech 25(2):149–162
7. Saikia G (2014) Extending modules for iCub simulator to emulate human grasp forms. In: Signal Processing and Integrated Networks (SPIN), 2014 International Conference on. IEEE, pp 636–640
8. Synek A, Settles M, Stillfried G (2012) Multi-body simulation of a human thumb joint by sliding surfaces. In: Biomedical Robotics and Biomechatronics (BioRob), 2012 4th IEEE RAS & EMBS International Conference on. IEEE, pp 379–384
9. Neves DR (2011) Desenvolvimento de modelos biomecânicos tridimensionais do membro superior: mão e cotovelo. Federal University of Minas Gerais, Minas Gerais, Brazil
10. Musiolik A (2008) Multibody model of the human hand for the dynamic analysis of a hand rehabilitation device. Universidade Tecnica de Lisboa
11. Xu S, Grande-Allen K (2010) The evolution of the field of biomechanics through the lens of experimental mechanics. Exp Mech 50:667–682
12. Semitela A, Fonseca F, Completo A (2020) Experimental evaluation of vertebral strain in lumbar total disc replacement. Exp Mech 60:119–128
13. Smith K, Gordon A (2017) Mechanical characterization of prosthetic feet and shell covers using a force loading apparatus. Exp Mech 57:953–966
14. Coimbra DFM (2011) O Tratamento da Rizartrose: Estado da Arte. Instituto de Ciências Biomédicas Abel Salazar
15. Santello M (2014) 2, Synergistic control of hand muscles through common neural inpu. In: Balasubramanian R, Santos VJ (eds) The human hand as an inspiration for robot hand development. Springer, Heidelberg, pp 23–48
16. Jarque-Bou NJ, Scano A, Atzori M, Müller H (2019) Kinematic synergies of hand grasps: a comprehensive study on a large publicly available dataset. J Neuroeng Rehabil 16:1–14
17. Choi Wh, Takeda Y (2020) Displacement analysis and design of a (2–RRU)–URR parallel mechanism performing 2R1T output motion for thumb rehabilitation. Robotics 9(3):67
18. Massy-Westropp C, Massy-Westropp N, Wechalekar H (2023) Normative values for pinch strength—relationship with joint hypermobility as measured with the Beighton criteria. J Hand Surgery Global Online 5(3):272–276
19. Ersin.: human skeletal and soft tissue meshes. GrabCAD, Tibial Intramedullary Nail (2023). Available at: https://grabcad.com/library/tibial-intramedullary-nail-1/details?folder_id=3126125. Accessed Feb 01 2023
20. Choset HM, Hutchinson S, Lynch KM, Kantor G, Burgard W, Kavraki LE et al (2005) Principles of robot motion: theory, algorithms, and implementation. MIT press
21. Mozgáslabor (2023) Main page of the OptiTrack motion lab of the MOGI department of BME. BME-MOGI MotionLab. Available from: https://motionlab.mogi.bme.hu/. Accessed 21 June 2023
22. Petró B, Kiss RM (2022) Validation of the estimated torques of an open-chain kinematic model of the human body. Period Polytech Mech Eng 66(2):175–182
23. Barroso PN, Nagem DAP, Miranda RJC, Kirkwood R, Pinotti M (2007) Quantitative Analysis of thumb range of motion during functional activities. 19th International Congress of Mech Eng 1:1–6
24. Ratner B (2009) The correlation coefficient: its values range between+ 1/- 1, or do they? J Target Meas Anal Mark 17(2):139–142
25. Dollar AM (2014) Classifying human hand use and the activities of daily living. The human hand as an inspiration for robot hand development, pp 201–216

Authors and Affiliations

A.F. Lemos[1,2] · L.A. Rodrigues da Silva[3] · B.V. Nagy[1] · P.N. Barroso[4,5] · C.B.S. Vimieiro[2,4]

✉ A.F. Lemos
alinefaria@mogi.bme.hu

L.A. Rodrigues da Silva
leonardo@ufsj.edu.br

B.V. Nagy
nagyb@mogi.bme.hu

P.N. Barroso
patriciabarroso@recuperarte.com.br

C.B.S. Vimieiro
claysson@gmail.com

[1] Department of Mechatronics, Optics and Mechanical Engineering Informatics, Budapest University of Technology and Economics, Műegyetem Rakpart, Budapest 1111, Hungary

[2] Graduate Program in Mechanical Engineering, Pontifícia Universidade Católica de Minas Gerais, R. Dom José Gaspar, 500, Belo Horizonte 30535-901, Minas Gerais, Brazil

[3] Department of Telecommunications and Mechatronics Engineering, Universidade Federal de São João del-Rei, Rod. MG 443, KM 7, Ouro Branco 36420-000, Minas Gearis, Brazil

[4] Graduate Program in Mechanical Engineering, Universidade Federal de Minas Gerais, Av. Antônio Carlos 6627, Belo Horizonte 31270-901, Minas Gearis, Brazil

[5] Clinic of Occupational Therapy and Physiotherapy, Recuperarte, Av. do Contorno, Belo Horizonte 30110-140, Minas Gearis, Brazil